Annals of the University of Petrosani, Electrical Engineering, 22 (2020)

THE LUENBERGER-PENG OBSERVER ANALYSIS FOR SENSORLESS VECTOR CONTROL SYSTEMS OF INDUCTION MOTORS

OLIMPIU STOICUTA[1]

Abstract: The article presents the analysis by numerical simulation in Matlab-Simulink of the rotor's flux Luenberger observer assembly coupled with a Peng speed observer. The proposed estimator is use in sensorless vector systems of induction motors.

Keywords: induction motors, sensorless vector control systems, observers.

1. INTRODUCTION

The dynamic performances of sensorless vector control systems depends on the accuracy of the online estimates made by the observers used.

The best-known observers used in sensorless vector control systems are extended Luenberger observer [10], [11], [12], extended Kalman filter [6], [8], MRAS observer [19], [22], extened Gopinath observer [14], [15], [21], MRAS speed observer coupled with rotor flux Gopinath reduced-order observer [7], [30], and Peng speed observer [17], [18] coupled with rotor flux Gopinath reduced-order observer [27].

The above-mentioned estimators are sensitive to changes in the electrical parameters of the induction motor and have stability problems in the area of very low operating speeds [3], [16], [22], [28].

Research in the last three decades in the field of sensorless vector control systems of the induction motor has focused on reducing the problems mentioned above, [20], [25], [26], [29]. In this regard, the article proposes a method for simultaneously estimating the speed, modulus and position of the rotor's flux phasor using a Luenberger rotor flux observer coupled with the Peng speed observer.

The proposed estimator is study in Matlab – Simulink. The article presents in detail the implementation in an S-Function block of the Luenberger observer, adapted according to the estimated speed with the Peng observer.

[1] *Associate Proffesor Eng. , Ph.D. at the University of Petroşani.*

2. MATHEMATICAL MODEL OF THE INDUCTION MOTOR

The equations defining the mathematical model of the induction motor are [1], [9], [16], [24], [32].

$$\frac{d}{dt}\begin{bmatrix}\underline{i}_s\\ \underline{\psi}_r\end{bmatrix}=\begin{bmatrix}a_{11} & a_{13}-j\cdot a_{14}\cdot z_p\cdot\omega_r\\ a_{31} & a_{33}+j\cdot z_p\cdot\omega_r\end{bmatrix}\cdot\begin{bmatrix}\underline{i}_s\\ \underline{\psi}_r\end{bmatrix}+\begin{bmatrix}b_{11}\\ 0\end{bmatrix}\cdot\underline{u}_s \tag{1}$$

$$\frac{d}{dt}\omega_r = H_{m3}\cdot M_e - H_{m2}\cdot\omega_r - H_{m3}\cdot M_f - H_{m3}\cdot M_r \tag{2}$$

where: $\underline{i}_s = i_{ds} + j\cdot i_{qs}$; $\underline{\psi}_r = \psi_{dr} + j\cdot\psi_{qr}$; $\underline{\psi}_r^* = \psi_{dr} - j\cdot\psi_{qr}$; $\underline{u}_s = u_{ds} + j\cdot u_{qs}$; $j=\sqrt{-1}$;

$$a_{11} = -\left(\frac{1}{T_s\cdot\sigma}+\frac{1-\sigma}{T_r\cdot\sigma}\right);\ a_{13}=\frac{L_m}{L_s\cdot L_r\cdot T_r\cdot\sigma};\ a_{14}=\frac{L_m}{L_s\cdot L_r\cdot\sigma};\ a_{31}=\frac{L_m}{T_r};\ a_{33}=-\frac{1}{T_r};$$

$$b_{11}=\frac{1}{L_s\cdot\sigma};T_s=\frac{L_s}{R_s};T_r=\frac{L_r}{R_r};\sigma=1-\frac{L_m^2}{L_s\cdot L_r};H_{m1}=\frac{3}{2}\cdot z_p\cdot\frac{L_m}{L_r};H_{m2}=\frac{F}{J};H_{m3}=\frac{1}{J};$$
$$M_e = H_{m1}\cdot\left(\psi_{dr}\cdot i_{qs}-\psi_{qr}\cdot i_{ds}\right)$$

In the mathematical model above, the following notations are used:

- $\underline{i}_s$ - stator current phasor; $\underline{\psi}_r$ - rotor flux phasor; $\underline{u}_s$ - stator voltage phasor; ω_r - induction motor rotor speed; M_r - load torque; M_e - electromagnetic torque; M_e - friction torque;
- electrical parameters: R_s, R_r - stator and rotor resistance; L_s, L_r - stator and rotor inductance; L_m - mutual inductance; T_s, T_r - stator and rotor time constant;
- mechanical parameters: J - rotor inertia; F - friction coefficient; z_p - number of pole pairs.

3. THE LUENBERGER-PENG OBSERVER

The equations that define the rotor flux Luenberger observer are [10],[11],[12]:

$$\frac{d\hat{x}}{dt} = A\cdot\hat{x} + B\cdot u + L\cdot C\cdot\left(y-\hat{y}\right) \tag{3}$$

where $\hat{x}=\begin{bmatrix}\hat{i}_{ds} & \hat{i}_{qs} & \hat{\psi}_{dr} & \hat{\psi}_{qr}\end{bmatrix}^T$; $u=\begin{bmatrix}u_{ds} & u_{qs}\end{bmatrix}^T$; $y=\begin{bmatrix}i_{ds} & i_{qs}\end{bmatrix}^T$;

$$A=\begin{bmatrix} a_{11} & 0 & a_{13} & a_{14}\cdot z_p\cdot\hat{\omega}_r \\ 0 & a_{11} & -a_{14}\cdot z_p\cdot\hat{\omega}_r & a_{13} \\ a_{31} & 0 & a_{33} & -z_p\cdot\hat{\omega}_r \\ 0 & a_{31} & z_p\cdot\hat{\omega}_r & a_{33} \end{bmatrix};\ B=\begin{bmatrix} b_{11} & 0 \\ 0 & b_{11} \\ 0 & 0 \\ 0 & 0 \end{bmatrix};\ C=\begin{bmatrix} 1 & 0 & 0 & 0 \\ 0 & 1 & 0 & 0 \end{bmatrix};$$

$$a_{11}=-\left(\frac{1}{T_s\cdot\sigma}+\frac{1-\sigma}{T_r\cdot\sigma}\right);\ a_{13}=\frac{L_m}{L_s\cdot L_r\cdot T_r\cdot\sigma};\ a_{14}=\frac{L_m}{L_s\cdot L_r\cdot\sigma};\ a_{31}=\frac{L_m}{T_r};\ a_{33}=-\frac{1}{T_r};$$

$$b_{11}=\frac{1}{L_s\cdot\sigma};T_s=\frac{L_s}{R_s};T_r=\frac{L_r}{R_r};\sigma=1-\frac{L_m^2}{L_s\cdot L_r}.$$

The coefficients of the Luenberger amplification matrix are:

$$L=\begin{bmatrix} la_{11} & -la_{12} \\ la_{12} & la_{11} \\ la_{21} & -la_{22} \\ la_{22} & la_{21} \end{bmatrix} \tag{4}$$

The elements of Luenberger matrix are [10], [11]:

$$\begin{cases} la_{11}=(1-k)\cdot(a_{11}+a_{33}) \\ la_{12}=z_p\cdot\hat{\omega}_r\cdot(1-k) \\ la_{22}=-\gamma\cdot la_{12} \\ la_{21}=(a_{31}+\gamma\cdot a_{11})\cdot(1-k^2)-\gamma\cdot la_{11} \end{cases} \tag{5}$$

where $\gamma=1/a_{14}$, and k is the proportionality factor between the eigenvalues of the estimator and the eigenvalues of the induction machine ($k>0$).

From relations (3) and (4) is observed that the matrices A and L adaptation according to the rotor speed, which is estimated with the Peng observer. The block diagram of the Peng observer is in Fig. 1.

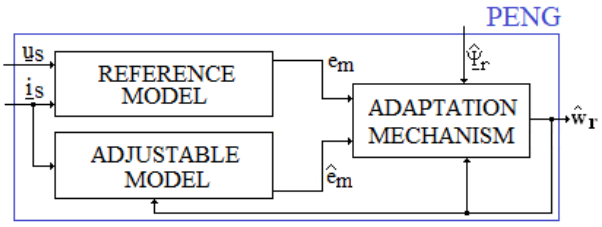

Fig. 1. The Peng speed observer

The following relations define the Peng speed observer [17], [18].

- The reference model

$$\underline{e}_m = \underline{u}_s - R_s \cdot \underline{i}_s - \sigma \cdot L_s \cdot \frac{d\underline{i}_s}{dt} \tag{6}$$

- The adjustable model

$$\underline{\hat{e}}_m = \frac{L_m^2}{L_r} \cdot \left(j \cdot z_p \cdot \hat{\omega}_r \cdot \underline{i}_m - \frac{1}{T_r} \cdot \underline{i}_m + \frac{1}{T_r} \cdot \underline{i}_s \right) \tag{7}$$

- The adaptation mechanism [18]

$$\hat{\omega}_r = k_p \cdot \varepsilon + k_i \cdot \int_0^t \varepsilon \, dt \tag{8}$$

where: $\underline{e}_m = e_{dm} + j \cdot e_{qm}$; $\underline{\hat{e}}_m = \hat{e}_{dm} + j \cdot \hat{e}_{qm}$; $\underline{i}_s = i_{ds} + j \cdot i_{qs}$; $\underline{i}_m = i_{dm} + j \cdot i_{qm}$;

$\varepsilon = \varepsilon_a + k_a \cdot \varepsilon_b$; $k_a = -T_r \cdot z_p \cdot \hat{\omega}_r$; $\varepsilon_a = \hat{\psi}_{dr} \cdot e_2 - \hat{\psi}_{qr} \cdot e_1$; $\varepsilon_b = \hat{\psi}_{dr} \cdot e_1 + \hat{\psi}_{qr} \cdot e_2$;

$e_1 = e_{dm} - \hat{e}_{dm}$; $e_2 = e_{qm} - \hat{e}_{qm}$.

In relation (7), $\underline{i}_m$ represent of the magnetization current phasor

$$\frac{d\underline{i}_m}{dt} = j \cdot z_p \cdot \hat{\omega}_r \cdot \underline{i}_m - \frac{1}{T_r} \cdot \underline{i}_m + \frac{1}{T_r} \cdot \underline{i}_s \tag{9}$$

In the above relationships $\underline{e}_m$ and $\underline{\hat{e}}_m$ is real and estimated induced back counter electromotive forces (e.m.f) phasors.

The block diagram of the Peng-Luenberger observer is in Fig. 2.

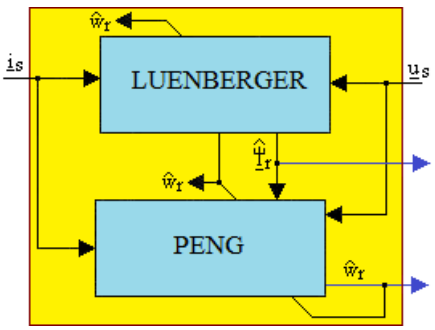

Fig. 2. The Peng-Luenberger observer

The adjustable model of Peng observer and Luenberger observer are adapted according to the estimated speed of the induction motor.

4. THE MATLAB-SIMULINK SIMULATION PROGRAM OF THE LUENBERGER-PENG OBSERVER

The Luenberger-Peng observer is study in Matlab – Simulink. The Matlab-Simulink simulation program of the Luenberger-Peng observer is in Fig.3.

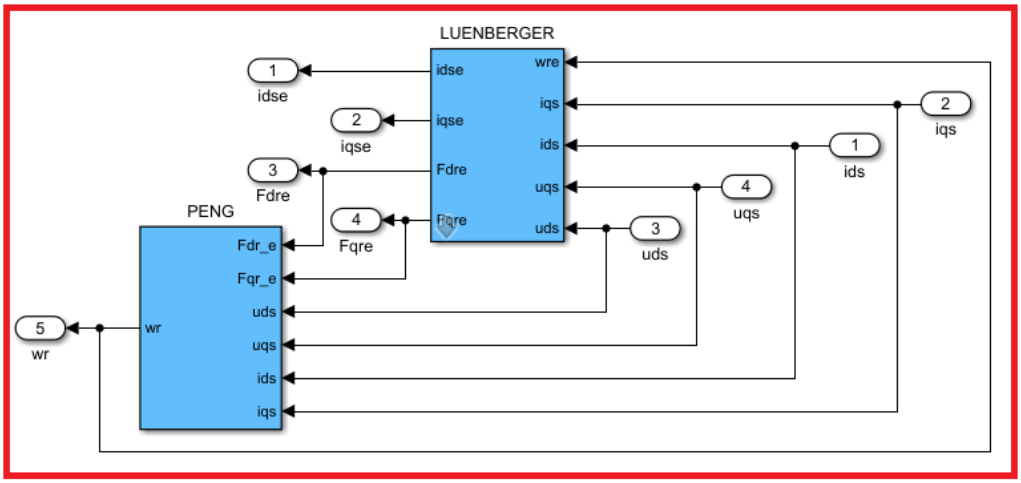

Fig. 3. The Matlab-Simulink simulation program of the Luenberger-Peng observer

The internal structure of the Peng observer is in Fig.4.

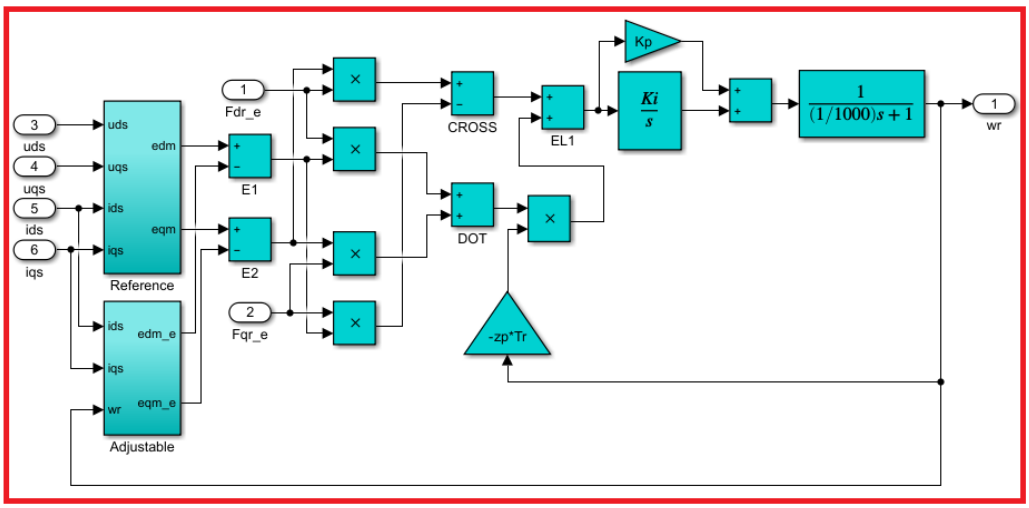

Fig. 4. The internal structure of the Peng observer

On the other hand, the reference model and the adjustable model from the Peng obsererver's component are in Fig.5

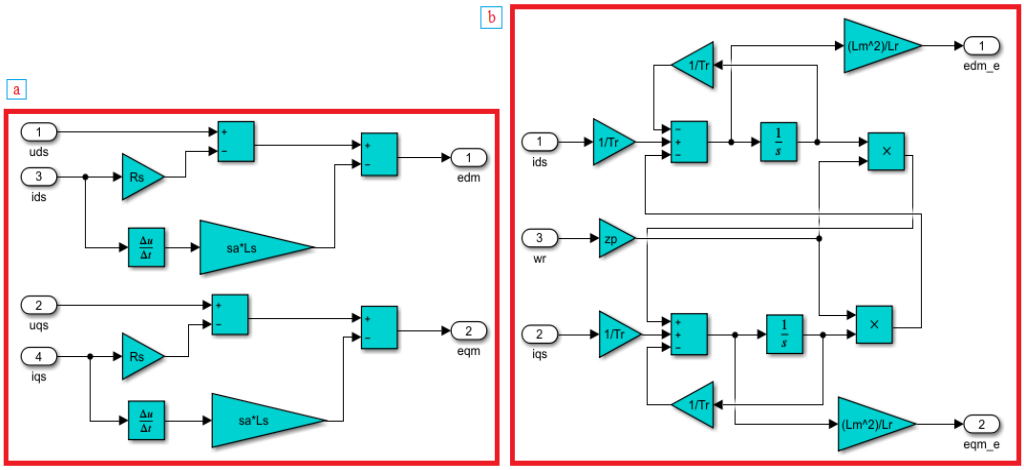

Fig. 5. The reference model (*a*) and the adjustable model (*b*) from the Peng observer.

The Luenberger observer is implemented in Matlab-Simulink based on an S-Function block [23], [24], [33]. The internal structure of the Luenberger block is shown in Fig.6.

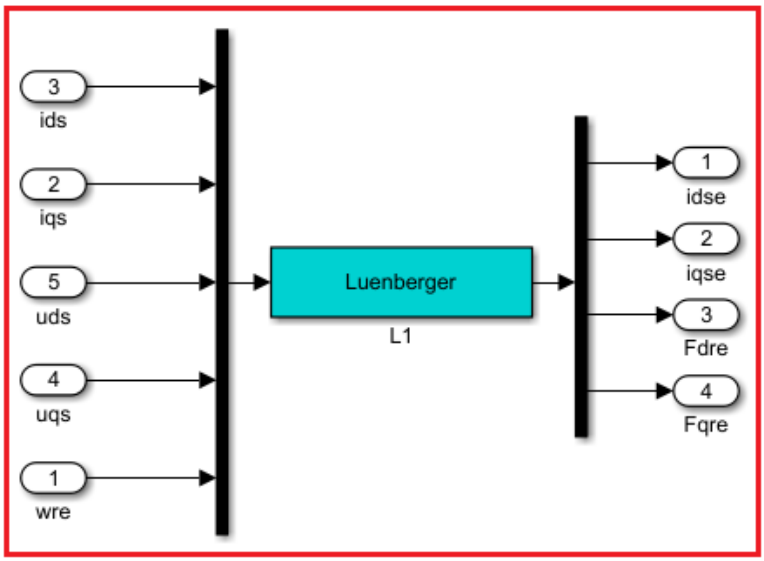

Fig. 6. Luenberger observer internal structure

The S-Function block which implements the Luenberger estimator is denoted "L1" in Fig.6.

The following figure shows the M-File code associated with this block.

```
function[sys,x0]=Luenberger(t,x,u,flag,zp,Rs,Rr,Ls,Lr,Lm)
k=1.2;
Ts=Ls/Rs;
Tr=Lr/Rr;
sa=1-(Lm^2)/(Ls*Lr);
a11=-1/(Ts*sa)-(1-sa)/(Tr*sa);
a13=Lm/(Ls*Lr*Tr*sa);
a14=Lm/(Ls*Lr*sa);
a31=Lm/Tr;
a33=-1/Tr;
b11=1/(Ls*sa);
ga=1/a14;
if abs(flag)==1
la11=(1-k)*(a11+a33);
la12=zp*u(5)*(1-k);
la22=-ga*la12;
la21=(a31+ga*a11)*(1-k^2)-ga*la11;
La=[la11 -la12;
    la12  la11;
    la21 -la22;
    la22  la21];
Aa=[a11  0    a13           a14*zp*u(5);
    0    a11  -a14*zp*u(5)  a13;
    a31  0    a33           -zp*u(5);
    0    a31  zp*u(5)       a33];
Ba=[b11  0;
    0    b11;
    0    0;
    0    0];
Xa=[x(1);x(2);x(3);x(4)];
Ua=[u(3);u(4)];
Ma=[u(1)-x(1);
    u(2)-x(2)];
sys=Aa*Xa+Ba*Ua+La*Ma;
elseif flag==3
   sys=x;
elseif flag==0
    sys=[4 0 4 5 0 0];
    x0=[0;0;0.001;0];
else
   sys=[];
end
```

Fig. 7. The M-File code of the “L1” block.

The estimated speed of the adaptation mechanism of the Peng observer is filtered through a low pass filter (see Fig. 4).

5. THE SIMULATION RESULTS

The Luenberger-Peng observer is tested by simulation in Matlab-Simulink within the sensorless vector control system, shown in Fig. 8.

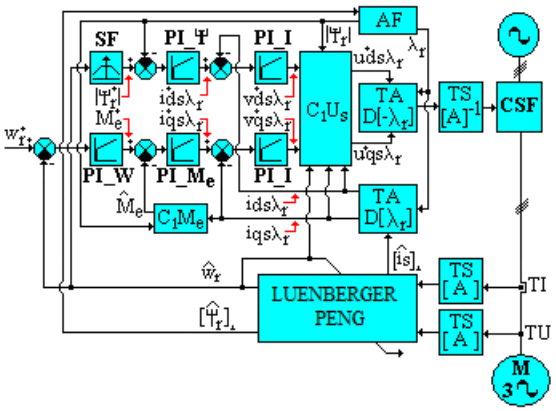

Fig. 8. The block diagram of the sensorless vector control system.

The main blocks within the vector control systems are defined by the following equations [16], [21], [25], [26], [27]:

- flux analyser (AF)

$$|\hat{\psi}_r| = \sqrt{\hat{\psi}_{dr}^2 + \hat{\psi}_{qr}^2}\,;\ \lambda_r = \operatorname{atan2}\left(\frac{\hat{\psi}_{qr}}{\hat{\psi}_{dr}}\right) \tag{10}$$

- the calculus of the torque block (C_1M_e)

$$M_e = \frac{3}{2}\cdot z_p \cdot \frac{L_m}{L_r}\cdot |\hat{\psi}_r| \cdot \hat{i}_{qs\lambda_r} \tag{11}$$

- stator voltages decoupling block (C_1U_s)

$$\begin{cases} u^*_{ds\lambda_r} = \dfrac{1}{b_{11}}\cdot\left[b_{11}\cdot v^*_{ds\lambda_r} - \left(a_{13}\cdot|\hat{\psi}_r| + a_{31}\cdot\dfrac{i^2_{qs\lambda_r}}{|\hat{\psi}_r|} + z_p\cdot\omega_r\cdot i_{qs\lambda_r}\right)\right] \\ u^*_{qs\lambda_r} = \dfrac{1}{b_{11}}\cdot\left[b_{11}\cdot v^*_{qs\lambda_r} + a_{14}\cdot z_p\cdot\omega_r\cdot|\hat{\psi}_r| + a_{31}\cdot\dfrac{i_{ds\lambda_r}\cdot i_{qs\lambda_r}}{|\hat{\psi}_r|} + z_p\cdot\omega_r\cdot i_{ds\lambda_r}\right] \end{cases} \tag{12}$$

- the field weakening block (SF)

$$\left|\psi_r^*\right| = \begin{cases} \dfrac{U_{\max}}{2\cdot\pi\cdot f_N} & \text{if} \quad \left|\hat{\omega}_r\right| \le \dfrac{2\cdot\pi\cdot n_N}{60} \\ \dfrac{L_m}{R_s}\cdot\dfrac{U_{\max}}{\sqrt{1+z_p^2\cdot T_r^2\cdot\hat{\omega}_r^2}} & \text{otherwise} \end{cases} \tag{13}$$

where: $U_{\max} = U_N \cdot \sqrt{\dfrac{2}{3}}$; U_N is the rated voltage; f_N is rated frequency; n_N [rpm] is the rated speed of the induction motor.

The five automatic controllers of the sensorless vector control system are Proportional Integral-type (PI) [13].

$$G(s) = K_n \cdot \left(1 + \frac{1}{T_n \cdot s}\right) \quad ; \quad n = 1,2,3,4,5 \tag{14}$$

The Matlab-Simulink simulation program of the sensorless vector control system is in Fig.9.

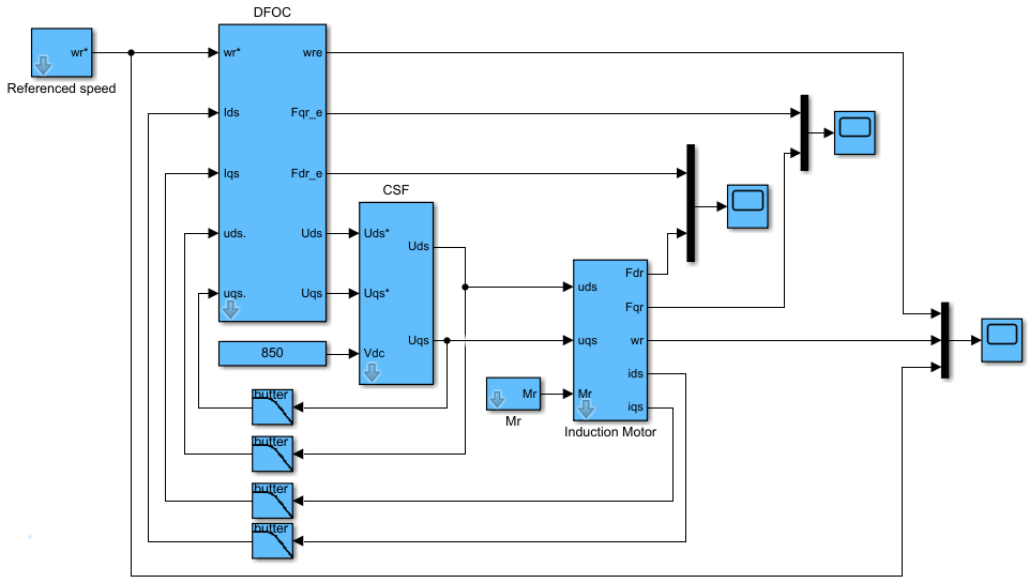

Fig. 9. The Matlab-Simulink simulation program of the sensorless vector control system

The transistors within the static frequency converter with intermediary continuous voltage circuit are considered of ideal commutation. Within simulation, the CSF disregards the mathematical models of the semiconducting devices.

Within the PWM modulator, the carrier is of isosceles triangle type having a frequency of 5 [kHz]. The modulation technique is based on a modified suboscillation method. This way, over the stator's reference voltages is injected the 3rd degree harmonic of the phase voltage, having amplitude of 1/6 of the fundamental reference voltage [5].

The sensorless vector control system are simulated in Matlab-Simulink using an induction motor of 4 [kW]. The electrical and mechanical parameters of the induction motor are given in the Table 1.

Table 1. Induction Motor Parameters

	Name	Value		Name	Value
R_s	*Stator resistance*	1.405 [Ω]	P_N	*Rated power*	4 [kW]
R_r	*Rotor resistance*	1.395 [Ω]	n_N	*Rated speed*	1430[rpm]
L_s	*Stator inductance*	0.178039 [H]	z_p	*Number of pole pairs*	2
L_r	*Rotor inductance*	0.178039 [H]	f_N	*Rated frequency*	50 [Hz]
L_m	*Mutual inductance*	0.1722 [H]	U_N	*Rated voltage*	400 [V] Y
J	*Motor rotor inertia*	0.0131[kg·m^2]	M_N	*Rated torque*	27 [N·m]
F	*Friction coefficient*	0.002985 [N·m·s/rad]	M_f	*Friction torque*	3.4 [N·m]

The internal structure of the control block with with direct orientation after rotor field (DFOC), is presented in Fig.10.

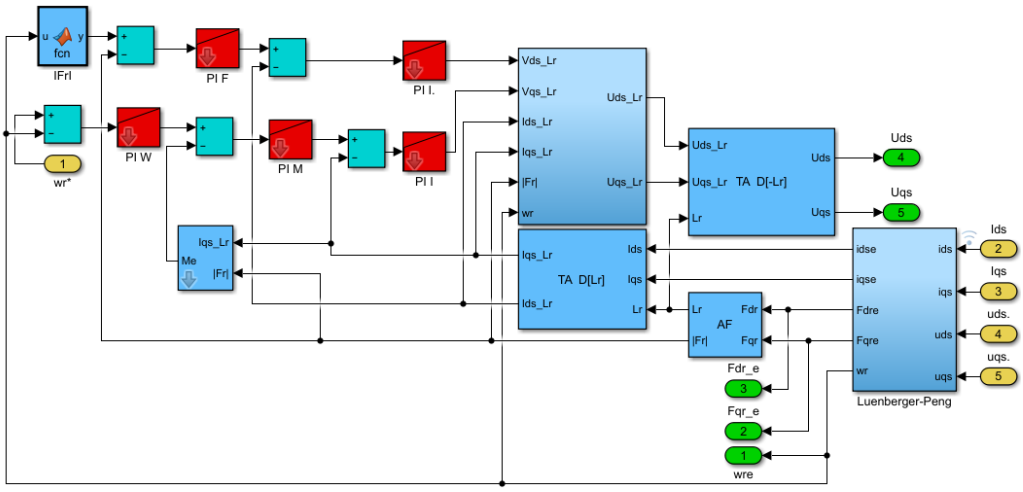

Fig. 10. The Matlab-Simulink program of the DFOC block

Because the first frequency which appears in the stator voltages spectrum is the triangular waveform frequency, both the currents and the stator voltages will be filtered with two pole Butterworth filters, which have de cutoff frequency set 500 [Hz].

The cutoff frequency of the filters is correlated with the frequency of the triangular signal within the inverter, in order to have an optimal aliasing.

The Dormand – Prince (ode45) method is used in the simulation, with a relative and absolute error of $\varepsilon = 10^{-6}$.

The rest of the constants used within the simulation are presented in Table 2.

Table 2. Simulation Parameters

	Name	**Value**	**Obs.**
K_1	*Parameter of proportionality*	370.5764	*The rotor flux controller*
T_1	*Time of integration*	0.1276	
K_2	*Parameter of proportionality*	0.0442	*The torque controller*
T_2	*Time of integration*	0.001	
K_3	*Parameter of proportionality*	0.8733	*The speed controller*
T_3	*Time of integration*	0.0298	
K_4; K_5	*Parameter of proportionality*	11.4865	*The current controllers*
T_4 ;T_5	*Time of integration*	0.0042	
k_p	*Parameter of proportionality*	462.6377	*Adaptation mechanism of Peng observer*
k_i	*Parameter of integration*	3624933	
k	*Parameter of proportionality*	1.2	*The Luenberger observer*

The simulated program from Fig.9, was compiled and ran on a numeric system operating Windows 10- 64b. The hardware structure of the system is built around an I7-4720HQ processor (2.6GHz), with 8 GB of available RAM.

The Luenberger-Peng Observatory was analyzed in two cases:

- *Case 1*. When the vector control system operates in the area of low speeds (60 rpm) and medium speeds (1000 rpm). In this case, the electrical parameters of the induction motor are unaltered.
- *Case 2*. When the vector control system operates in the area of low speeds (60 rpm) and medium speeds (1000 rpm). In this case, it is considered that the induction motor is preheated. As such, in the initial moment, the rotor resistance is considered with 5% higher than the rated value.

In simulation test when the vector control system operates at medium speeds (1000 rpm), the induction motor is functioning under load, having at its ax a load torque equal to that of the rated torque of the induction motor.

When the vector control system operates at low speeds (60 rpm), the induction motor is functioning under load, having at its ax a load torque equal to 5 Nm.

For each analyzed case, the time variation of the imposed, estimated and measured speed of the induction motor is highlighted, as well as the time variation of

the imposed, estimated and real rotor flux phasor module. The obtained results are presented in the following figures.

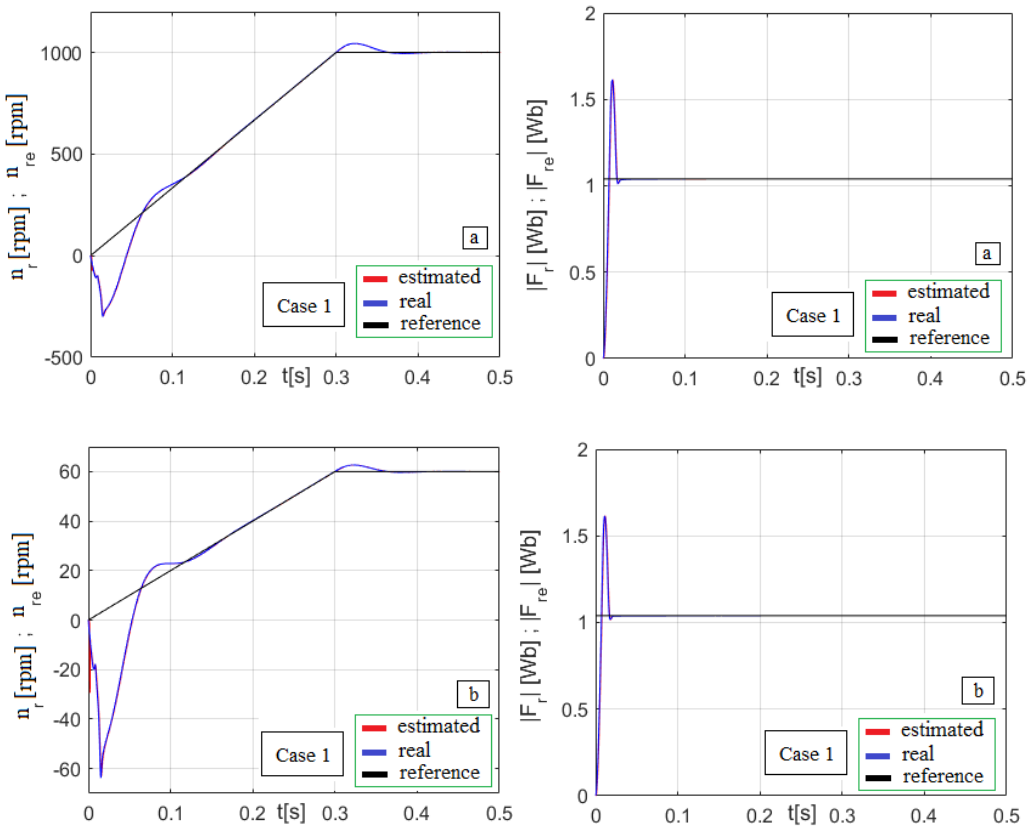

Fig. 11. Simulation results – Case 1

From the Fig.11, it is observed that the modulus of the rotor flux phasor is estimated very well, the stationary error being a very small one. In the transient period the estimated rotor flux phasor module has an overshoot of 54%. In the case of the rotor flux phasor modulus, the settling time is 0.03 [s].

On the other hand, from Fig.11 it is observed that the stationary error of the estimated/measured speed of the induction motor is a small one. Notable differences occur during the start of the induction motor. Disturbance (load torque) rejection time is approximately 0.15[s].

The maximum deviation of the estimated/real speed from the imposed speed when starting of the induction motor is 250 rpm (case 1.a), respectively 61 rpm (case 1.b). On the other hand, overshoot obtained at time 0.32 [s], is 4.5%. In the case of the speed, the settling time is 0.1 [s].

In order to obtain better transient dynamic performances two-degrees-of-freedom PI speed controllers with can be used [2], [4], [31].

The simulation results for case 2, are presented in Fig. 12.

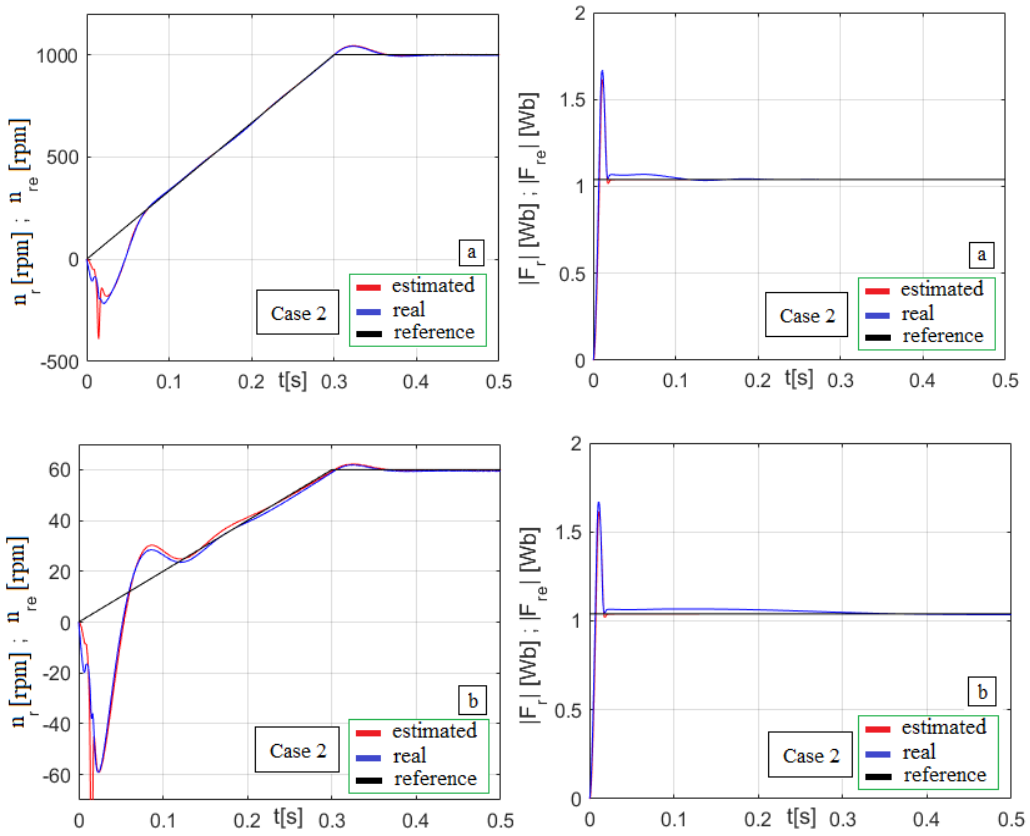

Fig. 12. Simulation results – Case 2

From the Fig.12, it is observed that the modulus of the rotor flux phasor is estimated very well, the stationary error being small one. On the other hand, in terms of the estimated rotor flux phasor modulus, the value of the overshoot is the same (54%). Notable differences in this regard occur in the case of the real rotor flux phasor module, in this case the overshoot increases, being 60%. In the case of the real rotor flux phasor modulus, the settling time is 0.15 [s] (case 2.a), respectively 0.35 [s] (case 2.b). In the case of the estimated rotor flux phasor modulus, the settling time remains the same (0.03 [s]).

On the other hand, the stationary error of the estimated speed of the induction motor is a small. Regarding the stationary error of the measured speed of the induction motor, this is about 2 rpm. Disturbance (load torque) rejection time is approximately 0.9 [s] (case 2.a), respectively 0.22 [s] (case 2.b).

The maximum deviation of the measured speed from the imposed speed when starting of the induction motor is 145 rpm (case 2.a), respectively 55 rpm (case 2.b).

On the other hand, the maximum deviation of the estimated speed from the imposed speed when starting of the induction motor is 340 rpm (case 2.a), respectively 227 rpm (case 2.b). The overshoot obtained at time 0.32 [s], is 4.1%. In the case of the speed, the settling time is 0.1 [s].

In this case, in order to increase the dynamic performances, a Luenberger-Peng observer can be made that adapts according to the rotor resistance.

6. CONCLUSIONS

Very good dynamic performances of the Luenberger-Peng observer make it a very good solution in sensorless vector control systems, when you want to estimate in tandem the speed, modulus and position of the rotor flux phasor of the induction motor.

Compared to the speed observer proposed by C. Schauder, the Luenberger-Peng observer has no problems with pure integration within the reference model.

Compared to the adaptation mechanism of the extended Luenberger observer (ELO) proposed by H. Kubota and adaptation mechanism of the MRAS observer proposed by C. Schauder, the Peng speed observer is more complex, requiring a number of more mathematical operations.

Following the tests performed, we can say that the Luenberger-Peng observer is less robust to the variation of the rotor resistance, compared to the ELO observer and the MRAS observer. This disadvantage can be eliminated by means of a Luenberger-Peng observer that adapts according to the stator resistance and the rotor resistance.

The simulation programs used to test the Luenberger-Peng observer are presented in detail offering a useful support for experts within automations and electrical engineering.

REFERENCES

[1]. **Boldea I., Nasar S.A.,** *Vector Control of AC Drives*, CRC Press, 1992.

[2]. **Gogea A., Stoicuta O., Pana T.,** *Comparative Analysis Between the PI Speed Controller and Two-Degrees-of-Freedom Speed Controller for Induction Motor Drive*, Proc. IEEE of MPS, Cluj-Napoca, Romania, pp.1-6, 2019.

[3]. **Gogea A., Stoicuta O., Pana T., Paramon A.,** *Comparative Study a Two Adaptive Observers of Speed and Rotor Flux of the Induction Motor*, 2019 8th International Conference on Modern Power Systems (MPS), Cluj Napoca, Romania, pp. 1-8, 2019.

[4]. **Harnefors L., Saarakkala S.E., Hinkkanen M.,** *Speed Control of Electrical Drives Using Classical Control Methods*, IEEE Transactions on Industry Applications, vol. 49, no. 2, pp. 889-898, 2013.

[5]. **Holtz J.,** *Pulsewidth Modulation for Electronic Power Conversion*, Proceedings of IEEE, vol.82, No.8, pp.1194 - 1214, 1994.

[6]. **Holtz J.,** *Sensorless Control of Induction Motor Drives*, Proceedings of IEEE, vol.90, No.8, pp.1359 - 1394, 2002.

[7]. **Hori Y., Umeno T.**, *Implementation of Robust Flux Observer based Field Orientation (FOFO) Controller for Induction Machine*s, Proc. IEEE of IAS Annual Meeting, San Diego, USA, pp.523-528, 1989.

[8]. **Kim Y.R., Sul S.K., Park M.H.**, *Speed Sensorless Vector Control of Induction Motor Using Extended Kalman Filter*, IEEE Trans. Ind. Application, vol.30, No.5, pp. 1225-1233, 1994.

[9]. **Kelemen A., Imecs M.,** *Field-Oriented AC Electrical Drives*, Romania Academy Publishing House, Bucharest, 1989.

[10]. **Kubota H., Matsuse K., Nakano T.,** *DSP-Based Speed Adaptive Flux Observer of Induction Motor*, IEEE Transactions on Industry Applications, vol. 29, No. 2, pp.344 - 348, 1993.

[11]. **Kubota H., Matsuse K.,** *Speed Sensorless Field-Oriented Control of Induction Motor with Rotor Resistance Adaptation*, IEEE Trans. Industry Application, vol. 30, No.5, pp. 1219–1224, 1994.

[12]. **Kubota H., Matsuse K.,** *Speed Sensorless Field Oriented Control of Induction Machines using Flux Observer*, Proceedings of IECON'94 - 20th Annual Conference of IEEE Industrial Electronics, Bologna, Italy, vol.3, pp. 1611-1615, 1994.

[13]. **Pana T, Stoicuta O.,** *Controllers Tuning for the Speed Vector Control of Induction Motor Drive Systems*, Proc. IEEE of AQTR, Cluj-Napoca, Romania, pp.1-6, 2010.

[14]. **Pana T., Stoicuta O.,** *Design of a new Adaptive Observer for Sensorless Induction Motor Drive*, Annals of the University of Craiova – Electrical Engineering, pp.73-78, 2010.

[15]. **Pana T., Stoicuta O.**, *Small Speed Asymptotic Stability Study of an Induction Motor Sensorless Speed Control System with Extended Gopinath Observer*, Journal of Advances in Electrical and Computer Engineering, vol.11, No.2, pp.15-22, 2011.

[16]. **Pana T., Stoicuta O.,** *Stability of the Vector Drive Systems with Induction Motors*, Mediamira Publishers, 2016.

[17]. **Peng F.Z., Fukao T.,** *Robust Speed Identification for Speed-Sensorless Vector Control of Induction Motors*, IEEE Trans. Ind. Application, vol. 30, No.5, pp. 1234-1240, 1994.

[18]. **Rashed M., Stronach A.F.**, *A Stable Back-EMF MRAS-Based Sensorless Low-Speed Induction Motor Drive Insensitive to Stator Resistance Variation*, IEEE Proc. Electr. Power Appl., vol.151, No.6, 2004.

[19]. **Schauder C.**, *Adaptive Speed Identification for Vector Control of Induction Motors without Rotational Transducers*, IEEE Trans. Ind. Application, vol.28, No.5, pp. 1054-1061,1992.

[20]. **Stoicuta O., Pana T.,** *Speed and rotor flux observer for sensorless induction motor drives*, Proc. of AQTR, Cluj-Napoca, Romania, pp.68- 73, 2012.

[21]. **Stoicuta O., Pana T., Molnar R.,** *Simultaneous Estimation of Speed and Rotor Resistance in the Sensorless Vector Control Systems with an Induction Motor, Based on Extended Gopinath Observer*, Acta Electrotechnica, vol.57, No.3, pp. 427-432, 2016.

[22]. **Stoicuta O., Pana T.,** *Asymptotic Stability Study of Induction Motor Sensorless Vector Control Systems with MRAS Observer*, Proc. IEEE of AQTR, Cluj-Napoca, Romania, pp.1-6, 2016.

[23]. **Stoicuta O.,** *The Utilization of the S-Function Block in Simulation of the Luenberger Rotor Flux Observer for Induction Motors*, Annals of the University of Petrosani – Electrical Engineering, No.18, pp.31-46, 2016.

[24]. **Stoicuta O.,** *The Utilization of the S-Function Block in Simulation of the Mathematical Model of Induction Motor with Iron Loss*, Annals of the University of Petrosani – Electrical Engineering, No.18, pp.5-20, 2016.

[25]. **Stoicuta O., Pana T., Molnar R., Deaconu D.,** *Simultaneous Estimation of Speed and Rotor Resistance in the Sensorless Vector Control Systems with Induction Motors*, 2017 International Conference on Electromechanical and Power Systems (SIELMEN), Iasi, pp.47-52, 2017.

[26]. **Stoicuta O., Pana T., Molnar R., Andras E.S., Deaconu D.,** *Online Compensation of Effects Caused of the Induction Motor Electrical Parameters Variations for Extended Luenberger Observer*, Bulletin of the Polytechnic Institute of Jassy, vol 64 (68), No.1, 2018.

[27]. **Stoicuta O., Pana T.,** *Comparative Study Between Extended Gopinath Observer and Back EMF-MRAS Speed Observer Coupled with Gopinath Rotor Flux Observer for Sensorless Vector Control of Induction Motor Drives*, 2019 International Conference on Electromechanical and Energy Systems (SIELMEN), Craiova, Romania, pp. 1-6, 2019.

[28]. **Stoicuta O., Pana T.C.,** *Asymptotic Stability Study of Induction Motor Vector Control Systems with Luemberger Observer*, 2008 IEEE International Conference on Automation, Quality and Testing, Robotics, Cluj-Napoca, pp. 242-247, 2008.

[29]. **Stoicuta O., Pana T.,** *New Adaptive Observer for Sensorless Induction Motor Drives*, Annals of the Univ. Eftimie Murgu of Resita, No.2, pp.175- 186, 2014.

[30]. **Tajima H., Hori Y.,** *Speed Sensorless Field Orientation Control of the Induction Machine*, IEEE Trans. Ind. Application, vol. 29, No.1, pp.175-180, 1993.

[31]. **Zaky M., Touti E., Azazi H.,** *Two-Degrees of Freedom and Variable Structure Controllers for Induction Motor Drives*, Advances in Electrical and Computer Engineering, vol.18, No.1, pp.71-80, 2018.

[32]. **Vas P.,** *Sensorless Vector and Direct Torque Control***,** Oxford Univ. Press, 1998.

[33]. ***********, *Simulink User's Guide, MathWorks, 2017.*